Supporting Information

Shida et al. 10.1073/pnas.1013728107

SI Materials and Methods

Antibodies. Polyclonal αTAT1 antibodies were raised in rabbits against purified full-length protein (Josman LLC) and affinity purified onto αTAT1[1-236] following standard protocols (1). Monoclonal mouse antibodies were against α-tubulin K40Ac (6-11B-1, Sigma), α-tubulin (DM1A, Thermo), and polyglutamylated tubulin (GT335, gift from Carsten Janke). Monoclonal rat antibody YL1/2 (Serotec) against tyrosinated α-tubulin was used in the immunofluorescence of Fig. 3 *A* and *E* and Fig. S3 and in the immunoblots of Fig. 3 *B* and *D*. Rabbit polyclonal antibodies were used to detect α-tubulin K40Ac (SA-452, Rockland; used in Fig. 4*C* and Fig. S3*B*); GFP (2); BBS4 (2), and Arl13b (3). Primary antibodies were diluted as indicated for immunofluorescence: 6-11B-1 (1:2,000), YL1/2 (1:500), GT335 (1:500), anti-Arl13b (1/150).

Primary antibodies were diluted as indicated for immunoblotting: 6-11B-1 (1:3,000), YL1/2 (1:2,500), GT335 (1:1,000), anti-αTAT1 (1 mg/mL), anti-BBS4 (1:250), and DM1A (1:1,000).

Secondary antibodies were diluted as indicated for immunofluorescence: Cy3-conjugated donkey antimouse (Jackson, 1:2,000), Cy5-conjugated donkey antirat (Jackson, 1:500), Alexa488-conjugated donkey antimouse (Invitrogen, 1:2,000), Cy3-conjugated donkey antirabbit (Jackson, 1:500).

For immunofluorescence of nematodes, 6-11B-1 was used at 1:200 and Alexa488-conjugated donkey antimouse (Invitrogen) was used at 1:5,000.

Secondary antibodies were diluted as indicated for fluorescent immunoblotting: DyLight800 goat anti-mouse (Thermo, 1:15,000), IRDye800 goat antimouse (LiCor, 1:15,000), and IRDye800 goat antirat (LiCor, 1:15.000).

For ECL-based immunoblotting, HRP-protein A (Invitrogen) was used at 1:10,000.

Immunoblotting. All immunoblots were developed with fluorescent secondary antibodies and visualized by infrared laser scanner (Odyssey, Licor), except for αTAT1 and GFP, which were developed with HRP-conjugated secondary antibodies and ECL. All fluorescent signals quantitated were within the linear range of the instrument.

Immunofluorescence Microscopy. Mammalian cells (Ptk2 and hTERT-RPE) were fixed with PFA/methanol (Fig. 4) or methanol (Fig. 3) and processed for immunofluorescence as described (4). *C. elegans* worms (N2, CB1607, GN232, GN233, and GN234) were fixed, permeabilized, and labeled with antibody as described (5). Briefly, animals were fixed in 2% paraformaledyde Ruvkun-Finney fixative (10 min), permeabilized using the peroxide tube fixation method (6) and stained with mAb 6-11B-1 and Alexa-488 secondary antibody.

All images were acquired on an Everest workstation (Intelligent Imaging Innovations) built around a AxioImager M1 (Zeiss) fitted with a CoolSNAP *HQ*^{2} CCD camera (Photometrics). The objective used was a PlanApo 63×/1.4 except for the montage in Fig. 5*A*, which was acquired with a PlanNeoFluar 10×/0.3.

DNA Constructs. Human αTAT1 cDNA (NM_024909) was used for all subcloning purposes. All αTAT1 variants (full length, mutants, and truncations) were subcloned into pGEX6P-DEST (bacterial expression) and into pEF5-GFP-DEST (mammalian transfections) by Gateway cloning. Sequences of all DNA constructs are available upon request.

C. elegans mec-17 and *atat-2* (W06B11.1) genomic sequences were obtained by PCR from WT (N2) genomic DNA, and cDNAs were obtained from the ORFeome collection (Open Biosystems). The *atat-2* promoter was a 3.14-kb fragment upstream of the predicted *atat-2* start codon amplified by PCR from genomic DNA. The *mec-17* promoter was 956-bp fragment upstream of the predicted *mec-17* start codon, amplified with the following primers. A *Patat-2*::mCherry construct was obtained by ligating the promoter fragment into a vector optimized for expression in *C. elegans*. The *Pmec-17* fragment was inserted in a Gateway destination vector to obtain mg#161. WT *mec-12* and *mec-17* cDNAs were inserted into mg#161 from the respective ORFeome vectors using the LR-clonase reaction. Mutations were introduced by site-directed mutagenesis (QuikChange, Stratagene). All cDNAs and promoter regions were verified by sequencing.

***C. elegans* Strains.** wild type (N2)
TU2769 *uIs31* III [*Pmec-17*::GFP]
CB1607 *mec-12(e1607)* III
RB1696 *mec-17*(*ok2109*) IV
RB1869 *atat-2*(*ok2415*) X
CX10 *osm-9*(*ky10*) IV
GN232 *mec-17(ok2109)* IV, outcrossed four times from RB1696 *mec-17(ok2109) IV*
GN233 *atat-2*(*ok2415)* X, outcrossed four times from RB1869 *W06B11.1(ok2415)* X
GN234 *mec-17*(*ok2109*) IV; *atat-2*(*ok2415*) X
GN235 *uIs31* III; *mec-17*(*ok2109*) IV
GN236 *uIs31* III; *atat-2*(*ok2415*) X
GN237 *uIs31* III; *mec-17*(*ok2109*) IV; *atat-2*(*ok2415*) X
GN238 *mec-12*(*e1607*) *uIs31* III
GN239 *mec-12*(*e1607*) III; *mec-17*(*ok2109*) IV; *atat-2*(*ok2415*) X
GN280 *mec-12*(*e1607*) III; *pgEx46* [*Pmec-17*::MEC-12(+), *Punc-122*::RFP]
GN283 *mec-12(e1607)* III; *pgEx49* [*Pmec-17*::MEC-12(K40R), *Punc-122*::RFP]
GN289 *mec-17*(*ok2109*) IV; *pgEx52* [*Pmec-17*::MEC-17(+), *Punc-122*::RFP]
GN292 *mec-17(ok2109)* IV; *pgEx55* [*Pmec-17*::MEC-17(D157N), *P*unc-122::RFP]
GN295 *mec-12*(*e1607*) III;*mec-17*(*ok2109*) IV; *atat-2*(*ok2415*) X
GN299 *mec-12*(*e1607*) III;*mec-17*(*ok2109*) IV; *atat-2*(*ok2415*) X; *pgEx61* [*Pmec-17*::MEC-12(K40Q), *Punc-122*::RFP]

RB1696 and RB1869 were obtained from the *C. elegans* knockout consortium and outcrossed four times to obtain GN232 and GN23. Both TU2769 and CB1607 were gifts from Martin Chalfie (Columbia University, New York) and were described previously (7, 8). CX10 was a gift from Cornelia I. Bargmann (Rockefeller University, New York). The deletion alleles *ok2109* and *ok2415* were confirmed by PCR with primers designed to span the predicted deletion plus an additional 1 kb of sequence 5′ and 3′ of the deletion. Double and triple mutants were made using standard genetic crosses.

Chemicals. All chemicals were purchased from Sigma unless otherwise indicated. Both [^{14}C]acetyl-CoA and [^{3}H]acetyl-CoA were purchased from Perkin-Elmer.

Recombinant Protein Expression and Purification. Proteins were expressed in *Escherichia coli* Rosetta2 after induction with 0.2 mM IPTG at 16 °C for 4 h. Proteins were bound to Glutathione Se-

pharose 4B and eluted into 2XT (40 mM Tris, pH 7.4, 400 mM NaCl, and 5 mM DTT) by overnight cleavage with PreScission protease (GE Healthcare). Due to the presence of degradation products, full-length αTAT1 was further purified by size exclusion chromatography on Superdex 200 developed in TBS (20 mM Tris pH 7.4, 150 mM NaCl, and 1 mM $MgCl_2$). The Stokes radius of full-length αTAT1 was calculated to be 3.5 nm based on its elution peak relative to calibration markers of known Stokes radii (thyroglobulin, 8.5 nm; IgG, 5.3 nm; ovalbumin, 3.05 nm; myoglobin, 1.87 nm; and vitamin B12, 0.75 nm). All proteins were aliquoted into single-use aliquots after addition of glycerol to 5%. Capture assays were performed as previously described (4).

Microtubule and BBSome Purification. Thrice-cycled and MAP-free bovine brain tubulin was purchased from Cytoskeleton or purified in the laboratory according to Weingarten et al. (9). *Tetrahymena* tubulin was purified from the outer doublet of axonemes as described (10). Microtubules were assembled by stepwise addition of taxol as described elsewhere (11). Analysis of pure tubulin polymerization and spindowns of cellular microtubules were conducted as previously described (12). The BBSome was purified by $Arl6^{GTP}$ affinity chromatography and MonoS cation exchange chromatography as described by Jin et al. (4).

Acetyltransferase Assays. Reactions were assembled in ADE buffer (40 mM Pipes, pH 6.9, 0.8 mM EGTA, 0.5 mM $MgSO_4$, 1 mM DTT) and contained 4.0 M glycerol (substrate saturation and truncation experiments: Figs. 1*F* and 2*C* and Fig. S1 *C* and *D*) or 1.6 M glycerol (all other figures) as well as 0.4 mM GDP (Fig. 2C, Tubulin saturation curve) or GTP (all other figures). All reactions were initiated by addition of acetylCoA to the following concentrations. Figs. 1 *B* and *H* and 2*A* and Fig. S1*A:* 16.7 μM [^{14}C]acetylCoA (60 mCi/mmol); Fig. 1*F*: 20 μM [^{3}H]acetylCoA (628 mCi/mmol); Fig. 2*B:* 50 μM [^{14}C]acetylCoA (50 mCi/mmol); and Fig. 2*C:* 20 μM [^{3}H]acetylCoA (628 mCi/mmol). The following reagent concentration were used except where otherwise noted: tubulin (12.5 μM), HAT1 (0.2 μM), RbAp46 (1.5 μM), histones H3/H4 (6.5 μM), and core histones (4.6 μM each). Reactions containing microtubules were assembled at RT, and all other reactions were assembled on ice. Reactions were stopped either by mixing 7.5-μL samples with SDS loading buffer or by filtering 5-μL samples on DEAE-cellulose filters (13). For phosphorimaging, 7.4-μL reaction samples were loaded into an SDS/PAGE well, and a 15-nL quantity was immunoblotted with the 6-11B-1 antibody directed against α-tubulin K40Ac. Phosphor screens were exposed for 4 d (Figs. 1 *B* and *H* and 2B and Fig. S1*A*) or 3 mo (Fig. 2*B*) and scanned with a Typhoon Trio (GE Healthcare). Filter-bound radioactivity was measured by scintillation counting, and the molar amounts of acetyl groups incorporated into tubulin were calculated after measuring the specific activity of [^{3}H]acetyl-CoA in the reaction.

Cell Culture, Transfection, and Analysis of Ciliation. Ptk2 cells were cultured in DMEM, reverse transfected with Fugene 6 while plated at 400 cells/mm^2, and fixed 48 h after transfection. RPE-hTERT cells were cultured, transfected, and serum starved as described elsewhere (4). For the siRNA transfection experiments, cells were reverse transfected and plated at 250 cells/mm^2 (Fig. 3 *C–H*) or 500 cells/mm^2 (Fig. 4) and 48 h after transfection, cells were either fixed (Fig. 3*E*) or switched from 10% to 0.2% FBS and fixed after the indicated time points (Fig. 4 and Fig. S3). Proliferation assays were performed by plating cells in 15-mm wells 48 h after siRNA transfection and detaching at each time point before counting.

siRNA-Mediated αTAT1 Depletion. All siRNAs were obtained from Qiagen (#2: SI04145162; #3: SI03124660; AllStars negative Control: 1027280). The siRNA sequences are as follows: αTAT1#2: 5′-ACCGCACCAACTGGCAATTGA-3′; αTAT1#3: 5′-AACCGCCATGTTGTTTATATT-3. Knockdown of αTAT1 expression was measured with RT–quantitativePCR using the Maxima SYBR Green/ROX kit (Fermentas) with primers αTAT1f (5′-GGCGAGAACTCTTCCAGTAT-3′) and αTAT1r (5′-TTGTTCACCTGTGGGACT-3′).

Phylogenetic Analysis. αTAT1 orthologs were identified by reciprocal BLASTP searches. When we failed to identify an ortholog by BLASTP, TBLASTN was used to search the available genome sequences. The correlation coefficient was calculated identically to that in Carvalho-Santos et al. (14).

Generation of Transgenic *C. elegans* Strains. Stable transgenic *C. elegans* strains were obtained by injecting the desired DNA construct (1 μg/μL) and a cotransformation marker (*Punc-122*::RFP, 10μg/μL) into the gonad of parental worms. Transgenic animals were recovered from their progeny according to the expression of *P*unc-122::RFP, which labels the six coelomocytes with red fluorescent protein. At least three independent transgenic lines were analyzed for each construct; there was no detectable difference in the behavior of these lines when assayed blind to genotype. For clarity, the data shown here were drawn from a single transgenic line for each transgene.

***C. elegans* Lysate Preparation.** Immunoblotting used the N2, CB1607, GN232, GN233, and GN234 strains. Whole-worm lysates were generated from washed worms immersed in BRB80 buffer (80mM Pipes, pH 6.8, 1 mM $MgCl_2$, 1 mM EGTA, 100 mM KCl, and protease inhibitors), quick-frozen in liquid nitrogen, and ground into a fine powder. The protein concentration of thawed lysates were measured using the Bradford assay. Proteins were separated on a polyacrylamide gel, transferred to nitrocellulose, and probed with the 6-11B-1 mAb directed against K40Ac α-tubulin.

***C. elegans* Behavioral Assays.** Nose touch and body touch were tested and scored as described (15, 16). In both assays, animals were subjected to 10 consecutive stimuli, and the number of responses was scored and reported. All behavioral assays were performed by an experimenter blind to genotype; at least 10 animals were tested in each day's trial and the results were compared across three trials conducted on different days.

Average speed was measured using the parallel worm tracker (17). Worms were tested on rectangular Petri dishes (3 × 6-cm, LabScientific), which carried a thin lawn of OP50 *E. coli* on one-half of their NGM surface. Animals placed on the food-free side and allowed to crawl toward the food-containing side of the assay plate. Tracks were divided into those collected from animals on the two sides of the plate and analyzed independently to obtain locomotion speed off and on food.

1. Harlow E, Lane D (1999) *Using Antibodies: A Laboratory Manual* (Cold Spring Harbor Laboratory Press, Cold Spring Harbor, NY).
2. Nachury MV, et al. (2007) A core complex of BBS proteins cooperates with the GTPase Rab8 to promote ciliary membrane biogenesis. *Cell* 129:1201–1213.
3. Cevik S, et al. (2010) Joubert syndrome Arl13b functions at ciliary membranes and stabilizes protein transport in Caenorhabditis elegans. *J Cell Biol* 188:953–969.
4. Jin H, et al. (2010) The conserved Bardet-Biedl syndrome proteins assemble a coat that traffics membrane proteins to cilia. *Cell* 141:1208–1219.
5. Cueva JG, Mulholland A, Goodman MB (2007) Nanoscale organization of the MEC-4 DEG/ENaC sensory mechanotransduction channel in Caenorhabditis elegans touch receptor neurons. *J Neurosci* 27:14089–14098.
6. Duerr JS (2006) Immunohistochemistry *WormBook*, ed. The *C. elegans* Research Community, WormBook. Available at http://www.wormbook.org.
7. Bounoutas A, O'Hagan R, Chalfie M (2009) The multipurpose 15-protofilament microtubules in C. elegans have specific roles in mechanosensation. *Curr Biol* 19: 1362–1367.

8. O'Hagan R, Chalfie M, Goodman MB (2005) The MEC-4 DEG/ENaC channel of Caenorhabditis elegans touch receptor neurons transduces mechanical signals. *Nat Neurosci* 8:43–50.
9. Weingarten MD, Suter MM, Littman DR, Kirschner MW (1974) Properties of the depolymerization products of microtubules from mammalian brain. *Biochemistry* 13: 5529–5537.
10. Reed NA, et al. (2006) Microtubule acetylation promotes kinesin-1 binding and transport. *Curr Biol* 16:2166–2172.
11. Elie-Caille C, et al. (2007) Straight GDP-tubulin protofilaments form in the presence of taxol. *Curr Biol* 17:1765–1770.
12. Loktev AV, et al. (2008) A BBSome subunit links ciliogenesis, microtubule stability, and acetylation. *Dev Cell* 15:854–865.
13. Borisy GG (1972) A rapid method for quantitative determination of microtubule protein using DEAE-cellulose filters. *Anal Biochem* 50:373–385.
14. Carvalho-Santos Z, et al. (2010) Stepwise evolution of the centriole-assembly pathway. *J Cell Sci* 123:1414–1426.
15. Hobert O, Moerman DG, Clark KA, Beckerle MC, Ruvkun G (1999) A conserved LIM protein that affects muscular adherens junction integrity and mechanosensory function in Caenorhabditis elegans. *J Cell Biol* 144:45–57.
16. Hart AC (2006) Behavior. *Wormbook*, ed The *C. elegans* Research Community, WormBook. Available at http://www.wormbook.org.
17. Ramot D, Johnson BE, Berry TL Jr., Carnell L, Goodman MB (2008) The Parallel Worm Tracker: A platform for measuring average speed and drug-induced paralysis in nematodes. *PLoS ONE* 3:e2208.
18. Hodges ME, Scheumann N, Wickstead B, Langdale JA, Gull K (2010) Reconstructing the evolutionary history of the centriole from protein components. *J Cell Sci* 123: 1407–1410.
19. Woodland HR, Fry AM (2008) Pix proteins and the evolution of centrioles. *PLoS ONE* 3: e3778.
20. Wickstead B, Gull K (2007) Dyneins across eukaryotes: A comparative genomic analysis. *Traffic* 8:1708–1721.
21. Manton I, Kowallik K, von Stosch HA (1970) Observations on the fine structure and development of the spindle at mitosis and meiosis in a marine centric diatom (Lithodesmium undulatum). IV. The second meiotic division and conclusion. *J Cell Sci* 7:407–443.

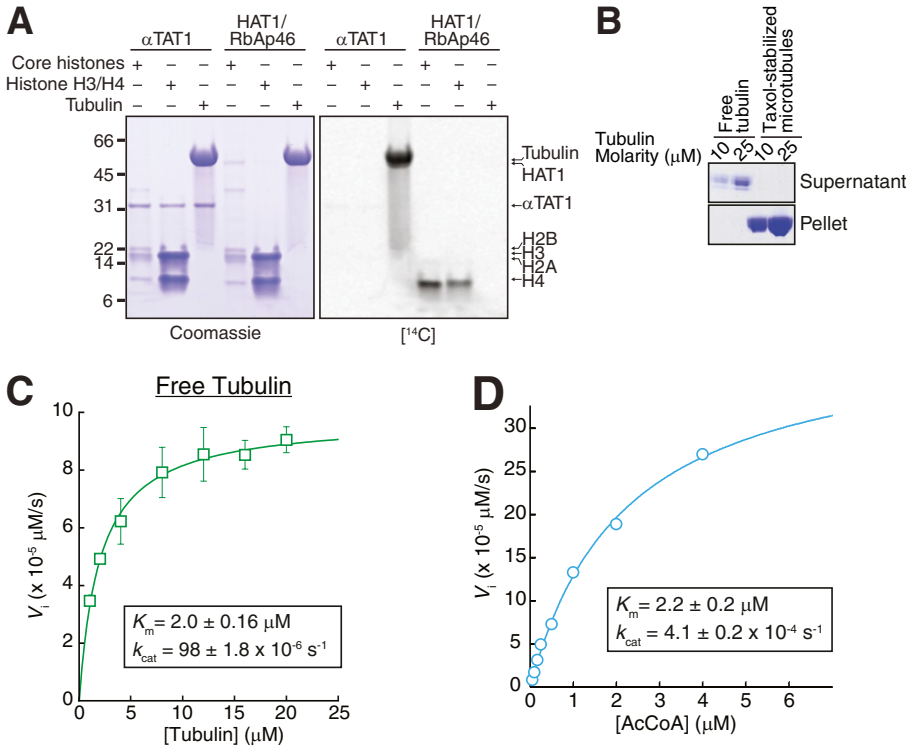

Fig. S1. αTAT1 specifically acetylates α-tubulin (*A*) αTAT1 exhibits a strict substrate specificity for tubulin vs. histones. The reaction mixtures contained 16.7 μM [^{14}C]acetylCoA (60 mCi/mmol) and various combinations of αTAT1[2-236] (4 μM), tubulin, HAT1/RbAp46 and histones H3/H4 and core histones and were incubated at 30 °C for 1 h. Neither histones H3/H4 nor core histones are detectably acetylated by αTAT1 and HAT1 is unable to detectably acetylate tubulin. (*B*) Microtubule spindown assays were conducted at the end of the 30 min incubation shown in Fig. 2*C*. As expected, free tubulin does not contain any pelletable material, whereas all of the tubulin in the microtubule sample is in the pellet. (*C*) Magnified version of tubulin saturation curve from Fig. 2*C*. (*D*) Measurement of αTAT1 enzymatic parameters for acetyl-CoA. A range of [^{3}H]acetyl-CoA concentrations (60 Ci/mmol) straddling the K_m value were incubated for 30 min at 22 °C with 1 μM αTAT1, and tubulin and radiolabel incorporation were measured with the filter assay.

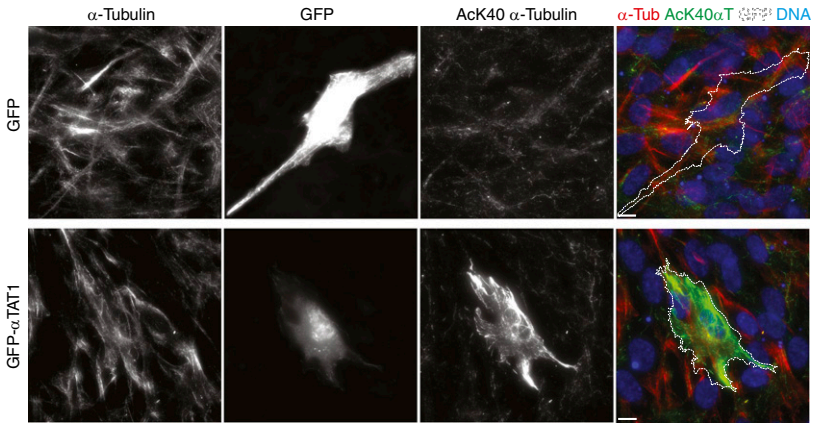

Fig. S2. Overexpression of αTAT1 in RPE-hTERT cells elevates the levels of α-tubulin acetylation at K40. RPE-hTERT cells were transfected as in Fig. 3*A*. (Scale bar, 10 μm.)

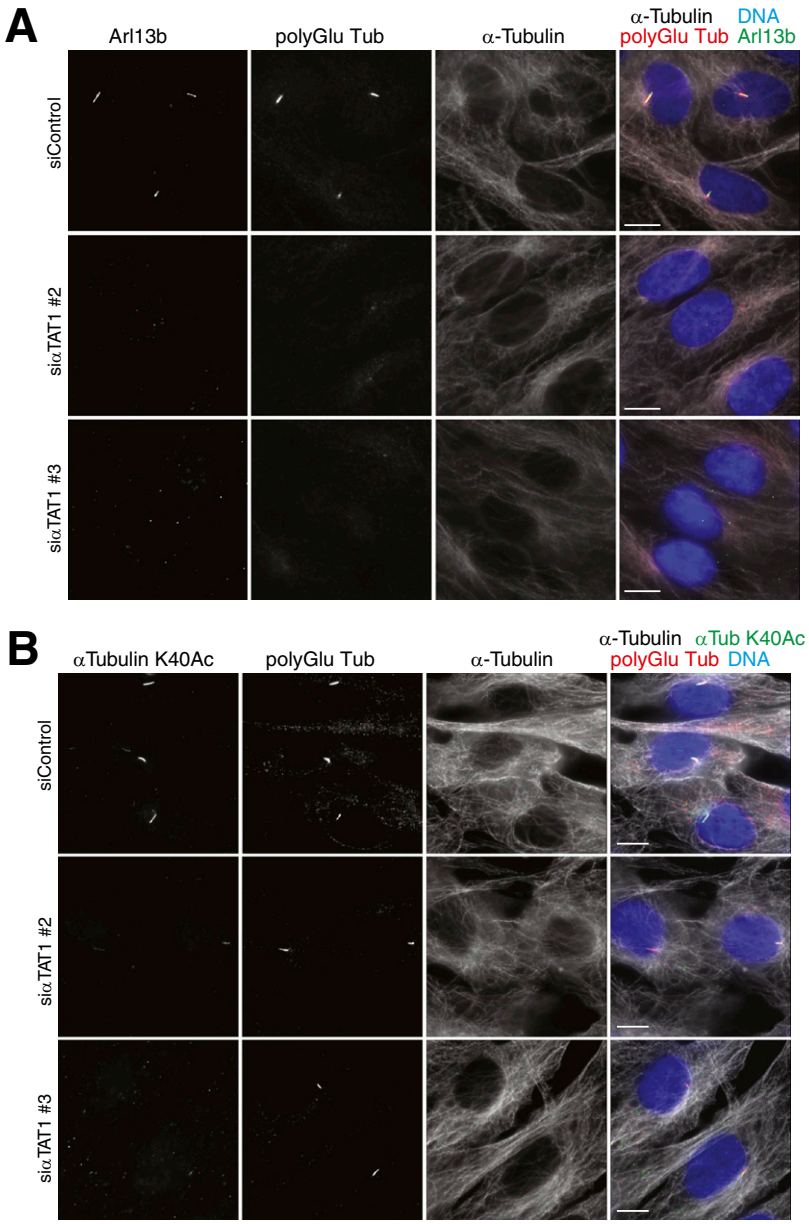

Fig. S3. αTAT1 promotes rapid assembly of the primary cilium and is required for α-tubulin acetylation at K40 in cilia. (*A*) Individual channels of panels shown in Fig. 4*B* are displayed with the addition of the αTAT1 siRNA #3 panel. Cells fixed 12 h after serum starvation were stained for polyglutamylated tubulin (red), Arl13b (green), α-tubulin (white), and DNA (blue). Note that although Arl13b and polyGlu tubulin are found in all cilia, polyGlu tubulin stains the proximal end of the axoneme and Arl13b staining extends all along the axoneme. (*B*) Individual channels of panels shown in Fig. 4*C* are displayed with the addition of the αTAT1 siRNA #3 panel. Cells fixed 24 h after serum starvation were stained for polyGlu tubulin (red), α-tubulin K40Ac (green), α-tubulin (white), and DNA (blue). A large proportion of cells are ciliated in the αTAT1-depleted cells; however, α-tubulin K40Ac staining in cilia of αTAT1-depleted cells is extremely faint.

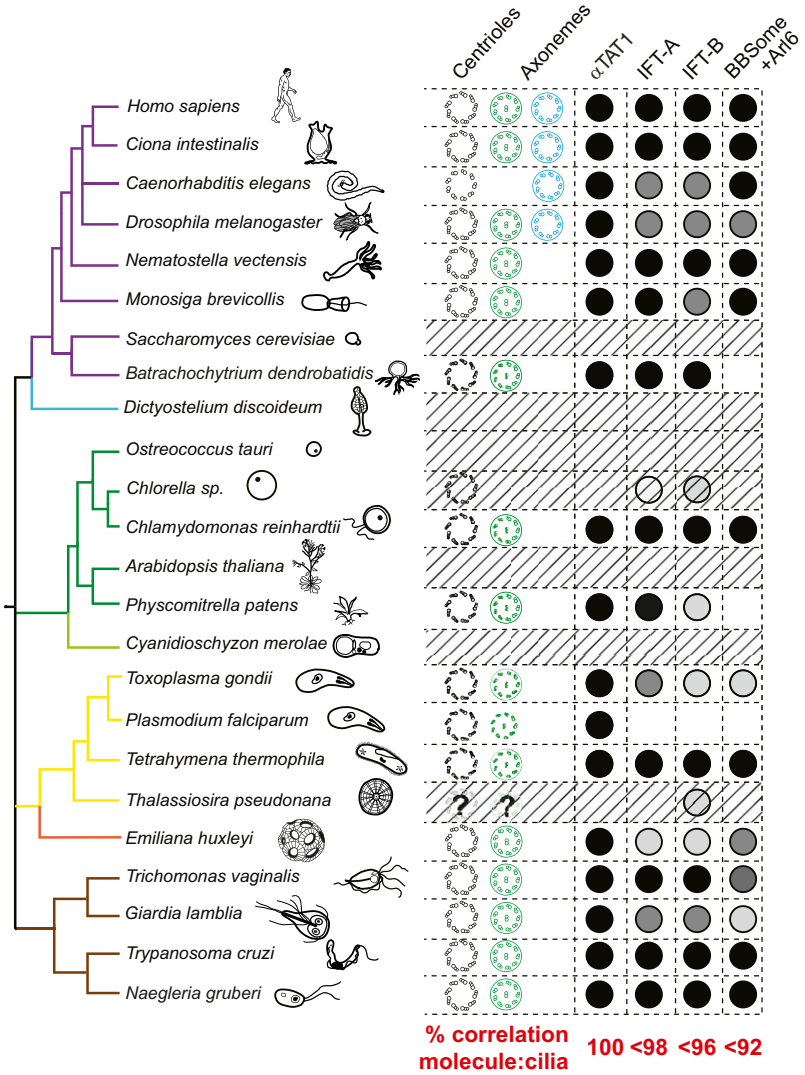

Fig. S4. Phylogenetic distribution of αTAT1 and the IFT-A, IFT-B and BBSome/Arl6 complexes. Simplified taxonomic tree representing crown eukaryotic groups in different colors [modified from Carvalho-Santos et al (14)]. Branch color code: purple, opisthokonts; blue, amebozoa; green, plants; yellow, alveolates and heterokonts; orange, haptophytes; and brown, excavates. When present in the organism, the basal body structure is diagramed in black and the cilium is shown in green (motile) or blue (primary). When no cilium is present, hatched bars fill the row. Membrane is omitted for *Plasmodium* cilium to represent IFT-independent flagellum assembly. Although other investigators have proposed that the centric diatom *Thalassiosira pseudonana* assembles a stubby flagellum at the gamete stage (14, 18–20) based on observation in distantly related centric diatoms (21), no gamete form of *T. pseudonana* has ever been reported despite decades of investigations, and this organism is likely to have lost the ability to assemble cilia. The presence of a αTAT1 ortholog is indicated by a black circle. Conservation of IFT-A and IFT-B complexes and of BBSome and Arl6 are depicted with black and shades of gray that correspond to the percentage of subunits for which orthologs are found (black, 100%; dark gray, <100%; medium gray, <60%; light gray, <30%).

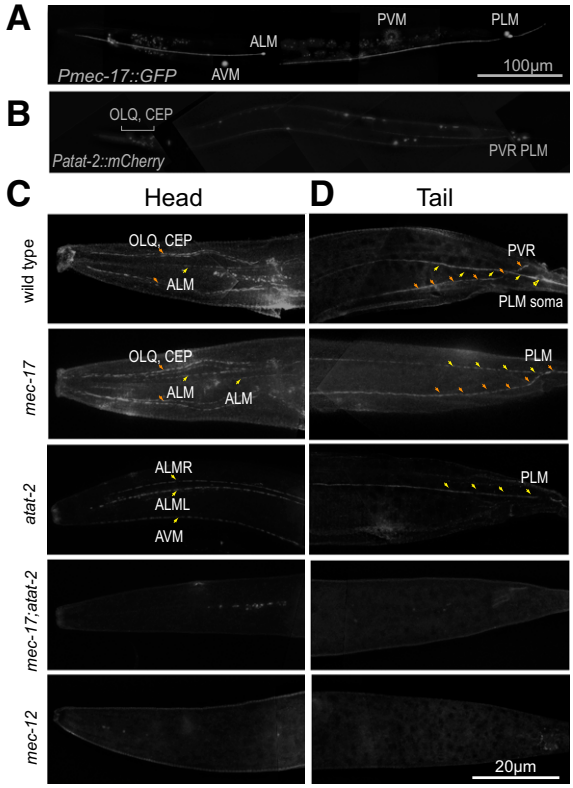

Fig. S5. Both *mec-17* and *atat-2* are expressed in a subset of neurons and are needed for αK40Ac in TRNs, OLQ, CEP, and PVR. (*A*) Fluorescent micrographs (montage) of transgenic animals expressing GFP under the control of the *mec-17* promoter. Only the six TRNs are labeled. (*B*) Fluorescent micrograph (montage) of transgenic animals expressing mCherry under the control of the *atat-2* promoter. OLQ, CEP, and PVR neurons are labeled in addition to the six TRNs. (*C* and *D*) Dependence of α-tubulin K40Ac expression on *mec-17*, *atat-2,* and *mec-12*. Immunofluorescence images of animals labeled with 6-11B-1 antibody: (*C*) heads; (*D*) tails. Loss of *mec-17* decreases TRN fluorescence, but has no apparent effect on signal in CEP, OLQ, and PVR, whereas loss of *atat-2* eliminates signal in CEP, OLQ, and PVR. Loss of both *mec-17* and *atat-2* eliminates all staining, as does loss of *mec-12,* a tubulin gene. Orange arrowheads indicate *atat-2*-expressing neurons; yellow arrowheads indicate *mec-17*-expressing TRNs.

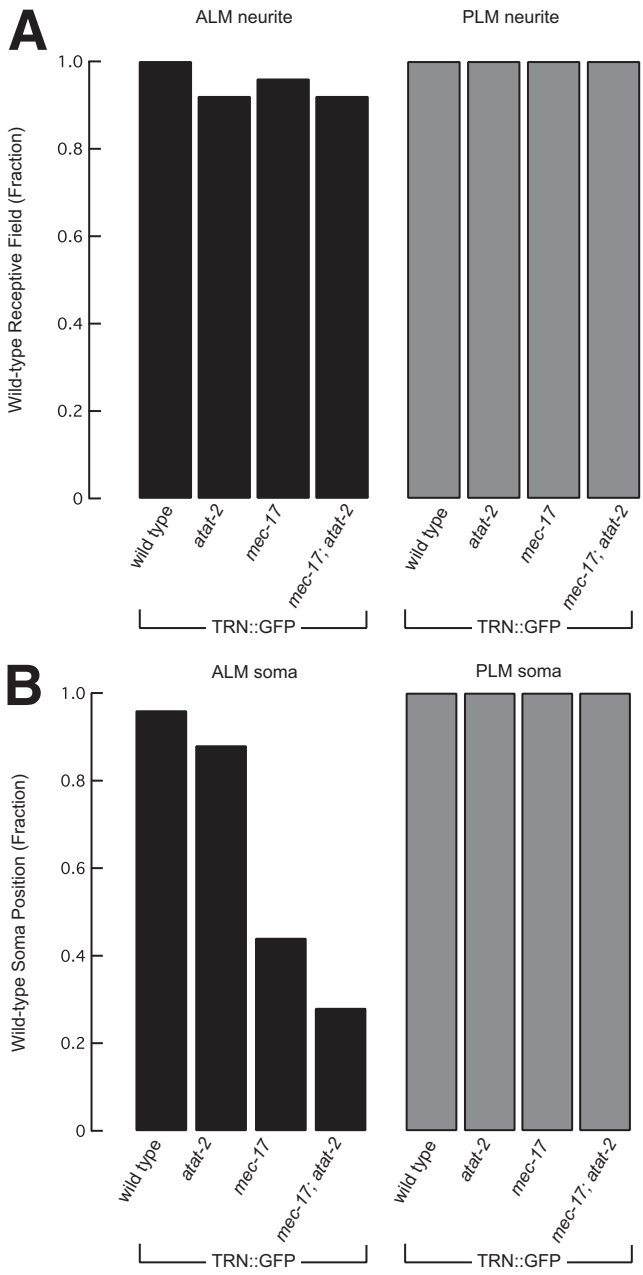

Fig. S6. Morphology of ALM and PLM in α*tat* mutant worms. (*A*) TRN neurite receptive field is essentially wild type. In WT animals, ALM's receptive field extends (anterior to posterior) from the tip of the nose to the vulva, and PLM's receptive field extends from the vulva to just posterior to the anus. (*B*) The PLM, but not ALM, somata are positioned normally in *tact* mutants. Both *mec-17* and *mec-17;atat2* mutant ALM somata are displaced anteriorly by ~2 μm (n = 25 young adult animals/genotype).

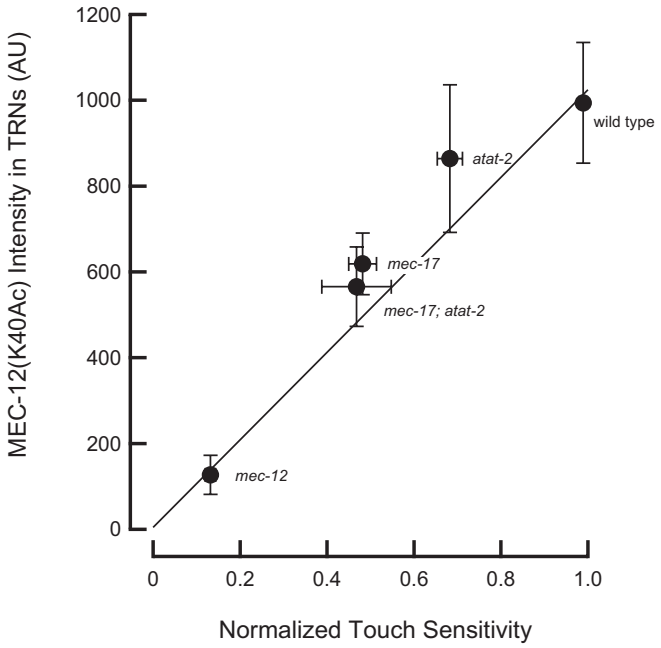

Fig. S7. Level of α-tubulin K40Ac in the TRNs is correlated with touch sensitivity. Points are mean ± SD of both measurements. At least 10 animals were analyzed for every genotype. Line is a linear fit to the data, with R^2 = 0.91. α-Tubulin K40Ac intensity was measured in PLM from background-subtracted images using ImageJ (National Institutes of Health). All micrographs were acquired at the same magnification and exposure time.

Dataset S1. Phylogenetic distribution of αTAT1 and all subunits of IFT-A, IFT-B, and BBSome complexes as well as Arl6

Dataset S1